Nanostructured Functional Layers for Solid Oxide Fuel Cells

A. Ansar*, D. Soysal, G. Schiller
German Aerospace Center (DLR), Stuttgart, Germany
*Syed-Asif.Ansar@dlr.de, Tel: +49 (0)711 6862 292, Fax: +49 (0)711 6862 747

Abstract

Nanostructured coatings are fabricated for potential use as electrodes in Solid Oxide Fuel Cells (SOFC) by developing innovative plasma spraying methods. The nanostructured NiO+YSZ anodes are fabricated by three means: spraying of pre-synthesized agglomerates of nanoparticles, suspension dc plasma spraying and solution precursor dc plasma spraying. Cathode deposits of variety of chemical composition having nanostructure were fabricated by thermal plasma chemical vapor deposition (TP-CVD) using RF-plasma torch. The deposits of desired phase and microstructure were successfully produced. The nanostructured anode, fabricated by pre-synthesized agglomerates of nanoparticles, exhibited better gas permeability, comparable high temperature conductivity, and 43% lower polarization in SOFC operation at 800°C compared to conventional anodes. Moreover, by controlling the electrode structure, the nanostructure of anode could be maintained for 1500 hrs of operation. Further improvement in the microstructure of anodes is in progress using dc plasma suspension and solution precursor spraying. Cathodes obtained from thermal plasma chemical vapor deposition (TPCVD) exhibited initially undesirable secondary phases which were overcome by adjusting the chemical composition of the precursors. The deposit columnar structure had high open porosity and specific surface area.

Keyword: SOFC, Nanostructured electrodes, plasma spraying, TPCVD, Suspension and solution precursor plasma spraying, electrochemical performance.

Introduction

Solid oxide fuel cells (SOFC), considered as highly efficient and environmentally friendly energy converters, convert chemical energy from fuel and oxidizing gases directly into electrical energy and heat [1]. The basic components of a SOFC cell consists of the porous electrodes, an anode for fuel supply and a cathode for air supply, which are separated by a gastight oxygen ion conductive electrolyte layer. The electrolyte is usually doped zirconia or ceria. A cermet consisting of yttria-stabilized zirconia (YSZ) and nickel is mostly used for the anode and perovskite-type oxides such as doped lanthanum manganite (LSM), lanthanum cobaltite and ferrite (LSC, LSF, LSCF) for the cathode are the common materials [2]. The electrodes have to provide the reaction sites for the oxidation of the fuel gas at the anode and for the reduction of oxygen molecules at the cathode. Ohmic, activation and concentration polarizations control collectively the performance of SOFCs. Resistivity in electrolyte has the main contribution to ohmic polarization. Activation polarization is dependent on electrodes-electrolyte interface and is controlled by charge transfer processes. Transport of gases (fuel and oxidizing) through electrodes governs concentration polarization. In case of thin film electrolyte cells, it has been observed that despite low ohmic polarization, the area specific resistance (ASR) of the cell could be several times larger which is due to much significant influence contributed by activation and concentration polarizations [3]. As suggested by different authors [4, 5], activation polarization can be effectively decreased by spreading of electrochemical reaction zone, i.e., as generally believed, the triple phase boundaries (TPBs) – interface of YSZ, Ni and fuel gas in the anode, and interface of YSZ, LSM and oxygen in the cathode. Electrodes having a microstructure that facilitates easy flow and homogeneous distribution of gases exhibit lower concentration polarization [6]. Significant improvement in electrode performance can be attained by introducing nanostructured materials which can

increase substantially the specific surface area and TPBs. However, tailoring the microstructure can be a challenge as the porosity and pore size needs to be adjusted to keep the concentration polarization limited. Additionally, several researchers have reported an increase of multiple orders of magnitude in the electronic and ionic conductivity at elevated temperatures for the nanocrystalline ceramics compared to solids having micrometric sized grains [7, 8].

Plasma spraying is one of the promising techniques to develop nanostructured functional layers for the SOFCs. It offers distinct advantages in terms of short fabrication time for the deposits, simple automation and up-scalability. In conventional plasma spraying, feedstock materials such as powders, wires etc, are introduced in a plasma jet using gas carrier. In the plasma, the particles are heated and accelerated simultaneously towards a prepared substrate. Impingement, flattening and solidification of impacted particles on the surface of a substrate results in lamellar structures, called splats. Consolidation of splats leads to construction of a deposit [9, 10]. The microstructure and quality of deposit depends on splat morphology and intersplat contact nature, which are influenced by substrate surface condition (temperature, roughness, chemical state, etc) [11] as well as impacting particle properties (temperature, velocity, Reynolds number (Re) and Webers number (We)) [12]. Feedstock and the operating conditions of plasma govern the in-flight properties of particles at impact. As the deposit is generated by random impact of particles on the substrate, microstructural control can be challenging. Additionally, feedstock material needs to have a momentum comparable to that of plasma gases at the injection for proper in-flight particle treatment. This is severe to fulfill for nanosized feedstock as the lower mass of particles needs to be compensated by higher velocities which tend to be too high for stable plasma. Our team is working towards developing innovative plasma spraying approaches to fabricate nanostructured deposit and an overview of these activities is described in this paper.

Nanostructured Anode using Agglomerated Nanoparticles

One of the methods consists of spraying nanoparticles agglomerated to coarse powder particles bigger than 10 µm. The feedstock powder for nanostructured anodes was produced by co-precipitation and spray drying of NiO and YSZ having a ratio of 22 to 78 weight%. The primary particles were 20 to 80 nm with d_{50} of 60 nm, calculated from XRD. The agglomerates had size range of -50+10 µm (Figure 1 (a)). To produce nanostructured anode deposit, this composite powder was co-sprayed along with an agglomerated micro-sized NiO powder. The NiO aggolerated were added to guarantee the percolation of Ni in anode. Air plasma spraying (APS) by a standard F4-type gun with a V-type 7 mm internal diameter anode nozzle from Medicoat, Switzerland was employed for deposition of anodes. The plasma enthalpy and particle velocity (governing particle dwell time in the plasma) were experimentally adopted to adjust spray parameters in such a way that only partial melting of the surface of agglomerated nano-powder occurred. This resulted in conserving the nanostructure during spraying. Powder carrier gas flow rate was adjusted to maintain a 3° deviation between the plasma and particle jet axis. The anode deposits were fabricated on porous FeCrMnTi substrates (48 mm in diameter, 1 mm in thickness), from Plansee, Austria. Figure 1 (b) presents the cross section of the nanostructured anode deposit. The as-sprayed deposits had particles raging from 60 nm to 220 nm measured randomly on several SEM micrographs at 1000X magnification. The characteristics of these nanostructured anodes were compared to our conventional NiO+YSZ anodes. The detail of processing of conventional anodes is described elsewhere [13]. Permeability of as sprayed and reduced anodes was measured with the pressure drop method where a constant transversal air flow causes a flow resistance or pressure drop through the anode layer and the coefficient of permeability (α) is recorded using the methodology and relationship described in [14, 15]. Higher α corresponds

to better permeability of gas through the layer. The data obtained for conventional and nanostructured layers are given in Figure 2. The conductivity of nanostructured and conventional anodes, measured by 4 point dc method at 800°C in Ar+5 vol% H_2, was comparable for 50 hours, as shown in Figure 3. An increase in the conductivity of nanostructured anodes was recorded for prolonged dwell times which was associated to coalescence and phase I sintering (neck formation) of Ni particles. Using impedance spectroscopy and equivalent circuit diagrams the polarization of conventional and a nanostructured anode was measured during SOFC operation at 800°C. The setup and details of measurements are described elsewhere [16]. In simulated reformat gas fuel (0.5 slm H_2 and 0.5 slm N_2), the polarization measured at open circuit voltage (OCV) associated to anode was decreased from 0.74 Ωcm² for conventional materials to 0.42 Ωcm² for nanostructured layer. Consequently the cell power density was increased from 230 mW/cm² to 309 mW/cm² after cell activation which typically takes 80 to 100 hours as shown in Figure 4. Please note that during initial 80 to 100 hours of cell operation, cells tested at DLR, show an improvement in OCV and decline in area specific resistance (ASR) leading to significant (almost twice) increase in cell out put power density. The effects, though not fully studied, are associated to the improvement in contacting, sealing and electrode-forming [17]. A reliable cell performance data is therefore reported after 100 hours. After 1500 hrs of operation a 5% decrease in the powder density was calculated. As the metal supported cells of DLR typically show degradation rates between 2.5 and 4.5% /kh [18], the 3.33%/kh degradation rates of cells consisting of nanostructured anode did not point towards any additional degradation linked to the use of nanomaterials. However, after 100 hours of operation, the nanostructured anode revealed neck formation and some densification, though the particle size remained comparable to that of as-sprayed coating which was between 60 and 220 nm, as shown in Figure 5 (a). In nanostructured anode operated for 1500 hours (Figure 5 (b)), limited particle growth was evident and random measurements on micrographs gave average particle size being 95 and 390 nm. This stability of the anode layer can be attributed to the distribution of YSZ and Ni particles inside the anode. While working with plasma sprayed deposits consisting of 40 nm 8YSZ, Christenn and Ansar [19] demonstrated that the phase I of sintering does not start in free standing deposits below 932°C at least for 60 hours and in constrained conditions, the sintering kinetics for nanostructured YSZ deposit are further slowed. Using these results, the nanostructured anode powder and deposit was prepared in a manner to limit percolation of nano-NiO particles. As a result, though the sintering at 800°C could not be eliminated, it was impeded due to the YSZ particles. The percolation of Ni is, however, mandatory for the electronic conductivity in anode and the micro-sized NiO was therefore added. Nevertheless, more work is needed to understand the grain growth of nanomaterials at cell operation conditions and the methodology to inhibit it.

Nanostructured Anodes using DC Suspension and Solution Precursor Plasma Spraying (SPS and SPPS)

Despite significantly better properties of deposits produced by spraying of agglomerated nanoparticles compared to conventional materials, the control of microstructure can be very challenging and the degree of porosity can only be tailored between 5 to 20%. Moreover, as the surface of each agglomerate needs to be melted for adhesion on the substrate, a large share of nanoparticles gets entrapped in the molten and re-solidified shell and does not contribute to the electrochemical activity of the electrodes. For functional deposits having denser or extremely porous structure of nanomaterials alternative methods are under development in our group. These methods consist of introducing nanoparticles as suspension, called suspension plasma spraying (SPS), or as precursor solutions, referred as solution precursor plasma spraying (SPPS), using DC plasma torches. Besides DLR, several groups have elaborated

activities in these processing techniques [20, 21, 22]. The former method uses nanoparticles dispersed in a solvent as feedstock. The preparation of this suspension is a crucial step of the process. Goal of the preparation is avoiding agglomeration of the particles to attain homogenous distribution of the particles required for constant feed rate and reduced sedimentation. As the Van-der-Waals forces are the major cause of the agglomeration, the suspensions are stabilized by promoting inter-particle repulsion by stearic or electro-static repulsion [23]. Zeta-potential (ς) is a common tool to measure the stability of suspensions. During the radial injection in the DC plasma, the solvent around the particles increases their momentum, as the mass of a droplet containing nanoparticles is several orders of magnitude higher than the mass of individual nanoparticle. This assist in delivering the particles till the core of the plasma jet. During the flight in the plasma jet, the solvent evaporates and releases the nanoparticles, which are then melted and accelerated towards the substrate. In solution precursor plasma spraying, a solution of the target material, usually nitrates, chlorates or sulfates, is injected into the plasma flame. Inside the flame the solvent evaporates and the precursor materials react and calcinate. Depending on the plasma process and operating conditions, deposit is generated either by growth from vapor phase or after melting and impingement of particles on the substrate. As both processes are based on injection of liquid feedstock, a very similar system can be used. In this work suspension plasma spraying was conducted by DC-TriplexPro gun from Sulzer Metco, Switzerland, using either atomizing or solid stream nozzles as shown in Figure 6.

The powders were nanosized 8YSZ and NiO from Marion Technology, France (Figure 7 (a)). The average particle size of 8YSZ was 35 nm whereas for NiO it was 92 nm. The suspensions were prepared in water using appropriate dispersants (Figure 7 (b)). Typical micrographs for very low and extremely high porosity are respectively shown in Figure 8 (a) and (b). Along with 45 nm particles in Figure 8 (b), a larger splat can be observed. It is believed to form when droplets trajectory is through cooler plasma zone causing slow evaporation of solvent. Agglomeration of nanoparticles thus takes place and the formed agglomerate then melts and impacts as single larger particle forming a splat with epitaxial crystals. For the dc solution precursor plasma spraying, aqueous solutions of zirconyl nitrate and yttrium nitrate from Alfa Aeser, France, were prepared. The ratio of the two components were adjusted to have 8 mole% Y_2O_3 in deposit. Solid loading was from 5 to 30 wt%. The solution was injected in TriplexPro gun using atomizing nozzle. The resulting coating was highly porous having cubic phase of zirconium oxide, checked by XRD (Figure 9).

Nanostructured Cathodes using RF-TPCVD

A promising approach for the preparation of SOFC components such as dense electrolyte and in particular porous cathode layers is given by the in situ synthesis and deposition in an inductively coupled RF plasma from liquid precursors. Using suspensions as well as aqueous solutions of suitable salts, two methods called RF-suspension plasma spraying (SPS) [24] and thermal plasma chemical vapour deposition (TPCVD) [25], have been developed for the deposition of SOFC components. The experiments were performed using a vacuum reactor and a PL50 induction plasma torch from TEKNA Plasma Systems, Sherbrooke/Canada which is operated with a radio frequency generator from Himmelwerk, Germany, at 500 kHz. The RF power was varied in the range from 20 to 30 kW, the chamber pressure was between 12 and 38 kPa and spraying distance between 150 and 600 mm. The plasma gas composition was varied over a wide range from argon/hydrogen mixtures to plasma mainly consisting of oxygen. The precursors were fed with a rate between 1.5 and 3 ml/min by a peristaltic pump using two channels to avoid pulsing. The material was directly injected into the hot plasma core by means of a gas-assisted atomizer. Argon flow rates in the range of 2-10 slpm were used to atomize the precursors. The schematic is shown in Figure 10.

Aqueous solutions of metal nitrates of different concentrations were used as precursors for the preparation of perovskite-type cathode coatings by means of TPCVD. A summary of the main precursor solutions applied and the desired synthesis products is given in Table 1. The phase content of the coatings was determined by XRD using a STOE Stadi P diffractometer and MoK_α radiation. Polished cross sections and fracture surfaces were prepared by standard metallographic procedures to study the coating microstructure by optical and scanning electron microscopy (SEM) as well as EDX mapping.

For first experiments, suspension plasma spraying was applied using suspensions of MnO_2 particles in saturated aqueous and ethanolic solutions of La salts [24]. The perovskite was formed as the main phase. However, La_2O_3 was also observed as an additional phase in significant extent in the coating. Post-treatment with an 80 % oxygen plasma improved the coating purity but the occurrence of detrimental La_2O_3 which reacts to $La(OH)_3$ causing severe volume change and destruction of the coating could not completely be suppressed. Furthermore, the coatings exhibit a layered microstructure resulting from impinging molten particles which is known from conventional thermal spraying processes. Although porosity can be affected by the solid content of the suspension SPS coatings showed a porosity which is too poor for gas migration in SOFC cathodes. Highly porous microstructures of LSM coatings were observed when using the TPCVD process, but the phase purity remained a problem to be solved [25]. A key parameter governing the purity of the coatings appears to be the radial temperature gradient within the plasma jet. When using lanthanum and manganese nitrates (precursors A, B, C), the high temperature along the axis of the jet combined with the high volatility of Mn results in a non-stoichiometric composition with regard to La and Mn in the central part of the coating on a stationary substrate. The deviations from stoichiometry are larger than the perovskite structure can tolerate, thus, the presence of surplus La causes La_2O_3 to appear in the coating beside the desired LSM phase. The cooler outer regions of stationary substrates were always covered with pure or almost pure perovskite phase. Figure 11 shows an extreme example of the different phase content obtained in the centre and in the outer region of a stationary substrate.

Scanning of the substrate results in the simultaneous deposition of the two main phases La_2O_3 and LSM. The homogeneity of the perovskite phase could be substantially improved by using precursors with lower lanthanum content, e.g. $La_{0.5}Sr_{0.5}MnO_3$ (precursors B and C) or by replacing lanthanum by praseodymium (precursor D), but a completely single-phase, large area perovskite coating could not be achieved. The synthesis of LSM, LSF (precursor E) and LSCF (precursor F) showed the same tendency concerning the formation of La_2O_3 but to a different extent. A semi-quantitative method was applied to compare the phase purity of different compounds by calculating the percentage of pure perovskite phase from the intensities of the main XRD peaks of the perovskite and La_2O_3. Table 2 depicts the phase composition of different perovskite layers. It is concluded that the volatility of the manganese cannot be the only reason for the non-stoichiometric incorporation of the elements into the central part of the perovskite coating. Regarding the melting points of the simple oxides of the considered elements, La_2O_3 and SrO show far higher values than the other oxides of Mn, Fe and Co. This leads to the consideration that clusters of La_2O_3 or La-Sr-oxide might form in the hot zone along the plasma jet by homogeneous nucleation similar to the observation made in the system with yttria-stabilised zirconia [25]. These clusters might then be deposited and cannot completely be transformed to the perovskite phase due to the limited interdiffusion of Mn, Fe and Co. A break-through concerning phase purity was achieved when using precursors where La is substituted by Pr (precursor H). With the slightly non-stoichiometric composition $Pr_{0.58}Sr_{0.4}Co_{0.2}Fe_{0.8}O_3$ (PSCF) absolutely pure perovskite phase could be observed by XRD measurement both in the centre and on the margin of the layer as can be seen from [25]. A description of the phase forming mechanisms can be found in [24, 25].

However, a complete explanation of this behaviour cannot be given at present and needs further investigation.
The coatings prepared from the precursor solutions A to H show a columnar or cauliflower-like microstructure as it is shown in SEM images of fracture surfaces in Figure 13, which is a result of heterogeneous nucleation of the material on the substrate surface as it is well known from conventional CVD. During growth of the perovskite layer needle-shaped single crystals are initially formed. The substrate is in a temperature range that provides enough surface diffusion of the impinging species. Therefore the needles can coalesce resulting in a columnar growth. The coalesced crystals were of size varying from 90 to 300 nm. The resulting microstructure is of high open directional porosity offering efficient vertical as well as horizontal gas migration paths. This is an ideal microstructure for application as SOFC cathode enabling excellent gas permeability and creating a lot of reaction zones. In order to create a composite cathode consisting of a mixture of YSZ and perovskite, YSZ has to be additionally formed in the plasma from an aqueous solution comprised of appropriate fractions of ziconyl nitrate and yttrium nitrate. Co-injection of both precursor solutions, i.e. one for the synthesis of pervoskite and other for YSZ, will be considered for the development of composite layers. The deposition of perovskite coatings by means of the TPCVD process from aqueous solutions resulted in growth rates of up to 25 µm/min on substrates with a size of 25 cm² that were scanned with the plasma jet. Depending on the process conditions and the precursor composition approximately 10 to 40 % of the theoretical oxide content of the precursors contributed to the coating growth. With optimization of the plasma parameters and application of larger substrates the deposition efficiency of the TPCVD process may achieve the range of about 100 µm/min which is typical for plasma sprayed ceramic coatings.

Conclusion

An overview of the advances in the plasma spraying processes was given to manufacture nanostructured functional layers for the application in the SOFCs. By introducing nanostructured deposits as electrodes in SOFC, improvement in their performance was attempted in term of the power density of cells while maintaining an acceptable degradation rates. Two major cost-effective approaches are here described. In the first one nanomaterials were pre-synthesized and introduced in plasma as agglomerates or suspensions whereas in the second method in-situ synthesis of the nanomaterials and nanostructured deposits was performed in the plasma jet using metal salts as precursors. The pre-synthesized nanoparticles were 40 to 90 nm and the size of the particles was mostly conserved after spraying; some portion was melted in-flight to provide adhesion on substrate which leads to incorporation of micro-sized particles. Plasma in-situ synthesized deposits have crystallite size varying between 95 to 390 nm. After electrochemical test and equivalent circuit diagram, it was found out that the nanostructured anode had 43.2% lower polarization (at OCV) in SOFC operation at 800°C with 0.5 slm H_2 and 0.5 slm N_2 mixture as fuel gas compared to conventional anodes. This led to and 34.5% higher power density for cells consisting of nanostructured anodes giving 309 mW/cm². Moreover, by controlling the electrode structure only limited growth in the nano-sized particles of anode was observed after 1500 hrs of operation at 800°C. In as-sprayed nanostructured anodes and anodes after 100 hours of operation, the particle size was between 60 and 220 nm, whereas it was between 95 and 390 nm after 1500 hours of operation. Further improvement in the microstructure of anodes is in progress using dc plasma suspension and solution precursor spraying. TPCVD cathodes initially exhibited undesirable secondary phases. This problem was overcome by adjusting the chemical composition of the precursors and controlling the thermally activated volatility of species during RF-plasma in-flight. The deposit microstructure was columnar type with very high open porosity and specific surface area which can offer excellent performance in SOFC.

Acknowledgment

The experimental work on TPCVD performed by Dr. Mathias Müller during the period of his PhD is gratefully acknowledged. The authors would also like to acknowledge Ms. Zeynep Ilhan for conducting the electrochemical tests.

List of Tables

Table 1: Summary of the precursor solutions applied and the desired synthesis products

	Synthesis product	Precursor	Concentration
A	$La_{0.9}Sr_{0.1}MnO_3$ (LSM)	$La(NO_3)_3 \cdot 6\ H_2O$ $Sr(NO_3)_2$ $Mn(NO_3)_2 \cdot 4\ H_2O$	0,9 M 0,1 M 1,0 M
B	$La_{0.5}Sr_{0.5}MnO_3$ (LSM)	$La(NO_3)_3 \cdot 6\ H_2O$ $Sr(NO_3)_2$ $Mn(NO_3)_2 \cdot 4\ H_2O$	0,5 M 0,5 M 1,0 M
C	$La_{0.65}Sr_{0.3}MnO_3$ (ULSM)	$La(NO_3)_3 \cdot 6\ H_2O$ $Sr(NO_3)_2$ $Mn(NO_3)_2 \cdot 4\ H_2O$	0,65 M 0,3 M 1,0 M
D	$Pr_{0.65}Sr_{0.3}MnO_3$ (UPSM)	$Pr(NO_3)_3 \cdot 5\ H_2O$ $Sr(NO_3)_2$ $Mn(NO_3)_2 \cdot 4\ H_2O$	0,65 M 0,3 M 1,0 M
E	$La_{0.8}Sr_{0.2}FeO_3$ (LSF)	$La(NO_3)_3 \cdot 6\ H_2O$ $Sr(NO_3)_2$ $Fe(NO_3)_3 \cdot 9\ H_2O$	0,8 M 0,2 M 1,0 M
F	$La_{0.8}Sr_{0.2}Co_{0.5}Fe_{0.5}O_3$ (LSCF)	$La(NO_3)_3 \cdot 6\ H_2O$ $Sr(NO_3)_2$ $Co(NO_3)_2 \cdot 6\ H_2O$ $Fe(NO_3)_3 \cdot 9\ H_2O$	0,8 M 0,2 M 0,5 M 0,5 M
G	$La_{0.58}Sr_{0.4}\ Co_{0.2}Fe_{0.8}O_3$ (LSCF)	$La(NO_3)_3 \cdot 6\ H_2O$ $Sr(NO_3)_2$ $Fe(NO_3)_3 \cdot 9\ H_2O$ $Co(NO_3)_2 \cdot 6\ H_2O$	0,58 M 0,4 M 0,8 M 0,2 M
H	$Pr_{0.58}Sr_{0.4}Co_{0.2}Fe_{0.8}O_3$ (PSCF)	$Pr(NO_3)_3 \cdot 5\ H_2O$ $Sr(NO_3)_2$ $Fe(NO_3)_3 \cdot 9\ H_2O$ $Co(NO_3)_2 \cdot 6\ H_2O$	0,58 M 0,4 M 0,8 M 0,2 M

Table 2: Phase purity of different TPCVD perovskite coatings

Precursor	ULSM		UPSM		LSCF		PSCF	
Position	centre	margin	centre	margin	centre	margin	centre	margin
Phase purity	85 %	100 %	92 %	100 %	65 %	100 %	100 %	100 %

List of Figures

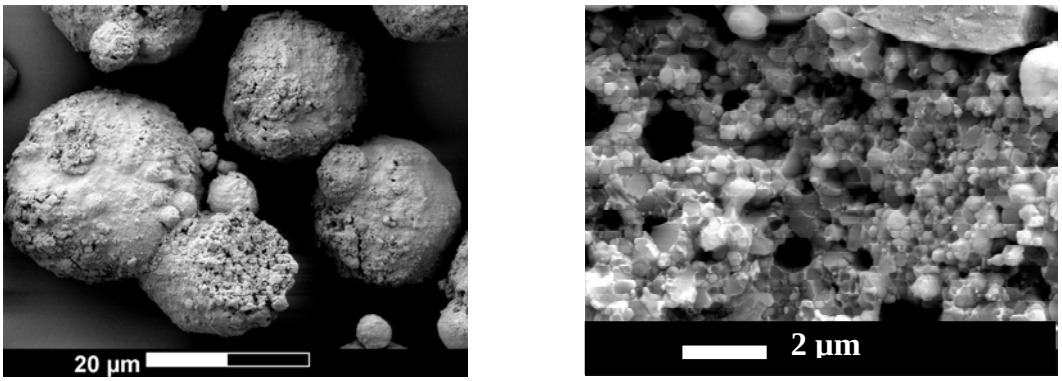

(a) (b)

Figure 1: SEM of the agglomerated nanostructured 22/78 wt% NiO and YSZ powder (a) and of the fractured cross section of the produced deposit after spraying of this powder.

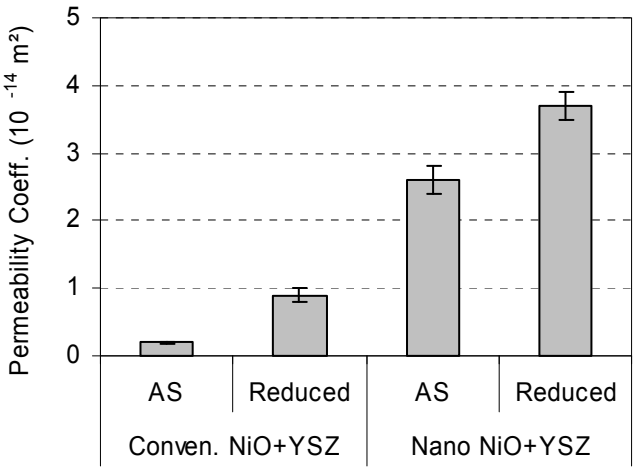

Figure 2: Comparison of permeability coefficient of conventional and nanostructured anodes.

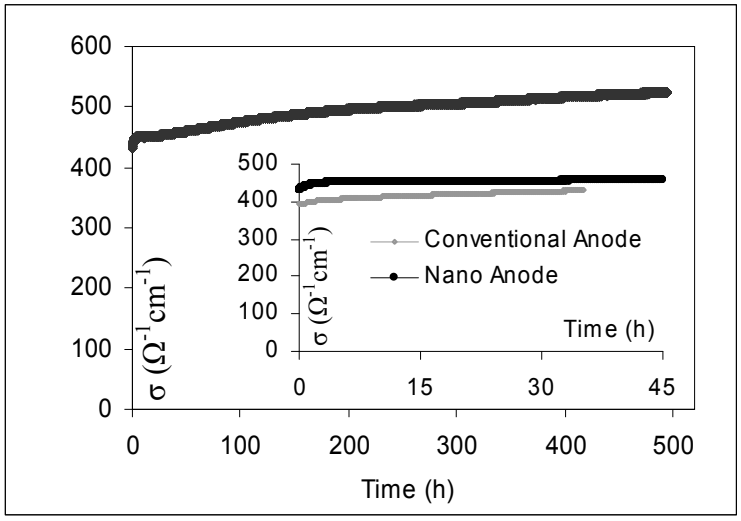

Figure 3: Conductivity of nanostructured anode in Ar- 5 vol% H_2 at 800°C as a function of time along with a comparison of conductivity of conventional and nanostructured anodes for 35 hrs. .

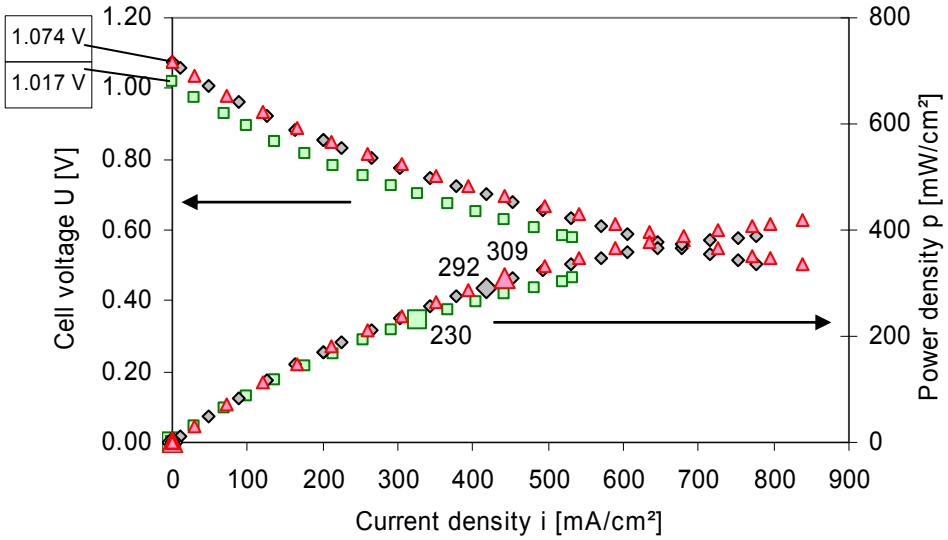

Figure 4: U(i) curves of reference cell (□), cell with nanostructured anode after 100 h (Δ) and after 1500 h of operation (◊) at 800°C (area 12.6 cm²; 0.5 slm H_2+0.5 slm N_2/2.0 slm air).

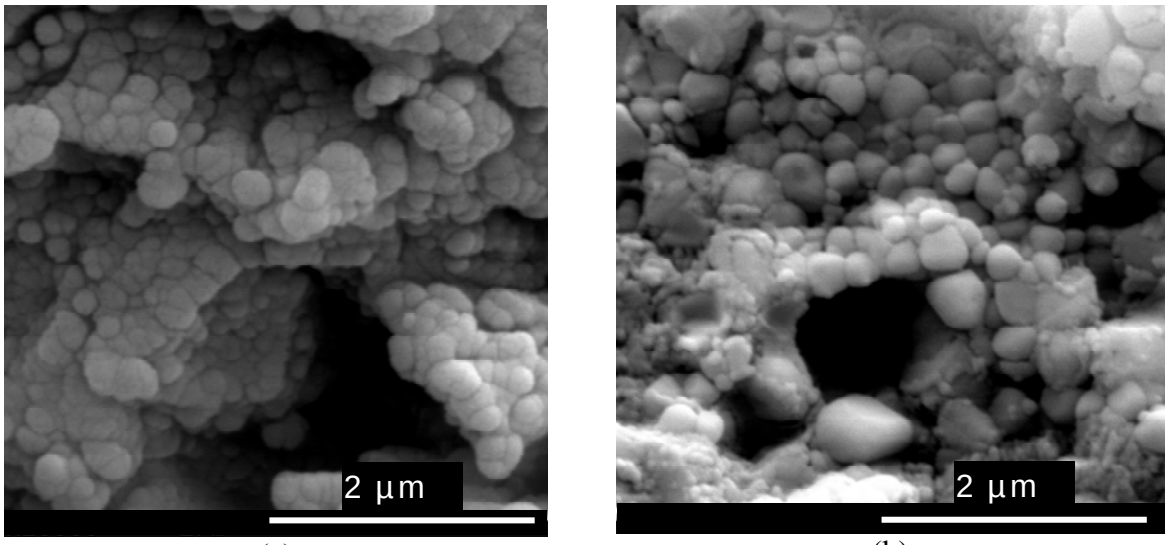

(a) (b)

Figure 5: SEM micrographs (2000X) of nanostructured anode after 100 h and 1500 h of SOFC operation. Micrograph (1000X) of as-sprayed deposit is given in Figure 1 (b).

(a)

(b)

Figure 6: Inverted photo of atomizing nozzle (a) and picture of liquid injection by a solid stream nozzle into plasma (b)

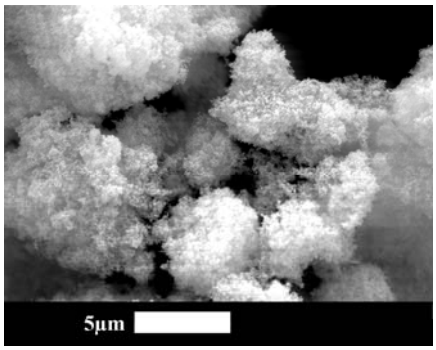

(a)

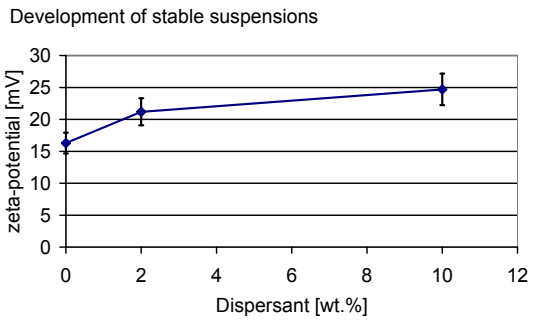

(b)

Figure 7: SEM image of the 8YSZ nanopowder (a) and typical zeta-potential measurement for suspension stabilization with increasing amount of dispersant (b).

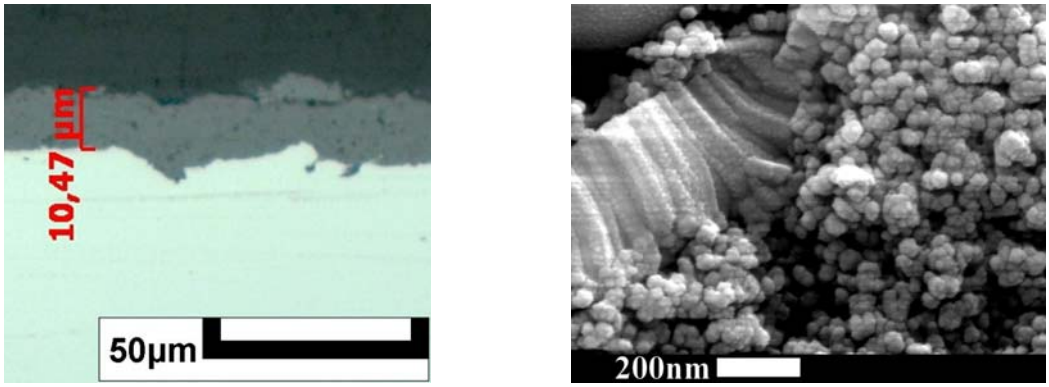

(a) (b)

Figure 8: Micrograph of thin dense (a) and highly porous (b) nanostructured YSZ deposits produced for SOFC by Suspension Plasma Spraying.

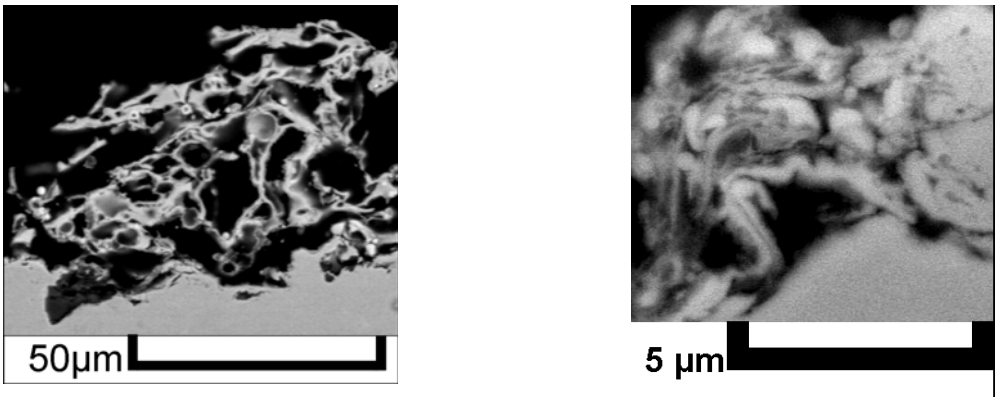

Figure 9: SEM images of porous zirconia layer by solution precursor plasma spraying.

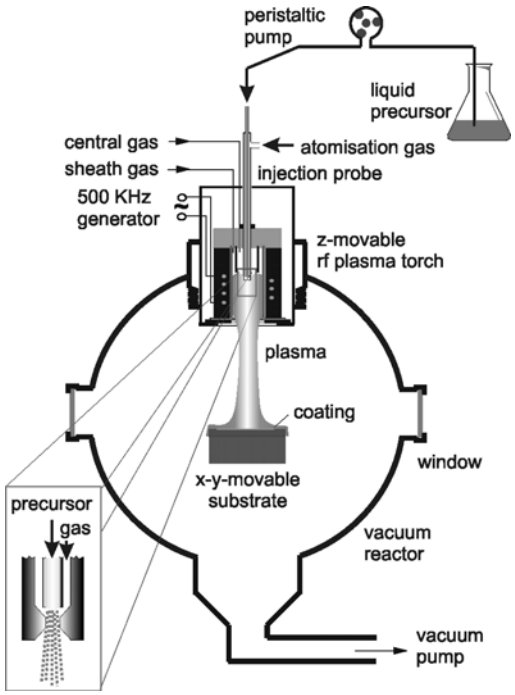

Figure 10: Experimental set-up, detail in left corner: principle of gas-assisted atomization

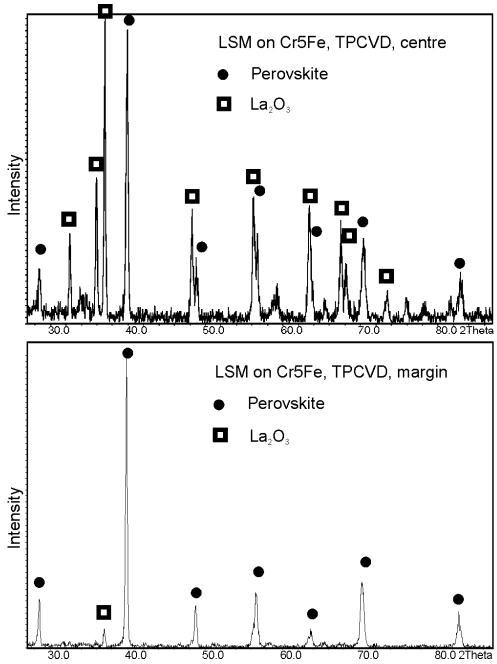

Figure 11: XRD patterns of a TPCVD coating of LSM (precursor A); top: centre, bottom: margin of the sample

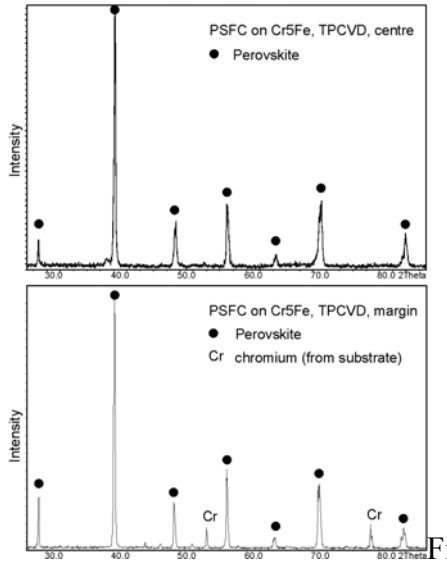

Figure 12: XRD patterns of a TPCVD coating of PSCF (precursor H), top: centre, bottom: margin of the sample.

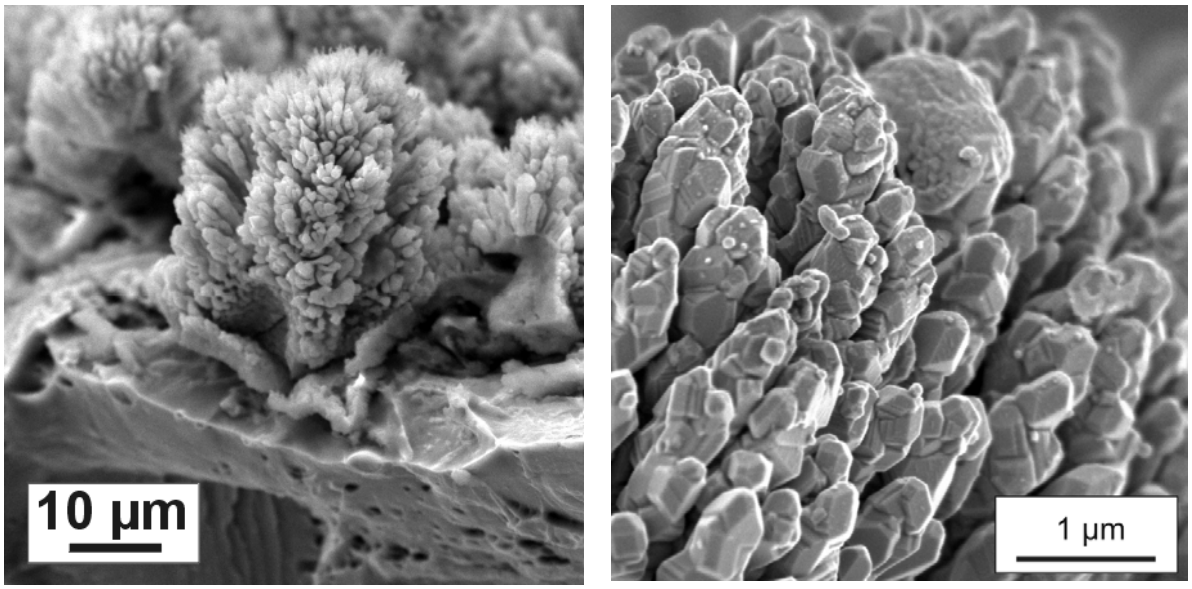

Figure 13: SEM images of a fracture surface of a TPCVD perovskite coating

References

1. S.C. Singhal, K. Kendall, High temperature solid oxide fuel cells: Fundamentals, design and applications, Elsevier 2003.
2. N.Q. Minh, T. Takahashi, Science and technology of ceramics fuel cells, Elsevier, 1995.
3. A.V. Virkar, J. Chen, C.W. Tanner, J.W. Kim, The role of electrode microstructure on activation and concentration polarization in solid oxide fuel cells, Solid State Ionics, 131, 2000, p. 189-198.
4. T. Kenjo, M. Nishiya, $LaMnO_3$ air cathodes containing ZrO_2 electrolyte for high temperature solid oxide fuel cells, Solid State Ionics, 57, 1992, p. 295-302.
5. H. Deng, M. Zhou, B. Abeles, Diffusion-reaction in mixed ionic-electronic solid oxide membranes with porous electrodes, Solid State Ionics, 74, 1994, p. 75-84.
6. A.A. Syed, Z. Ilhan, H. Weckmann, J. Arnold, G. Schiller, Improving plasma sprayed YSZ coatings for SOFC electrolytes, J. Therm. Spray. Technol., 2006, 15 (4), 2006, p 617-622.
7. H.L. Tuller, Ionic conduction in nanocrystalline materials, Solid State Ionics, 131, 2000, p 143-157
8. J. Maier, Nano-sized mixed conductors (Aspects of nano-ionics. Part III), Solid State Ionics, 148, 2002, p 367-374.
9. Thermal spraying, (pub.) American Welding Soc., Miami, USA, 1985.
10. Hand book of thermal spray technology, (ed.) J.R. Davis, (pub.) ASM International, USA, 2004.
11. A.A. Syed, A. Denoirjean, B. Hannoyer, P. Fauchais, P. Denoirjean, A.A. Khan, J:C. Labbe, Influence of substrate surface conditions on the plasma sprayed ceramic and metallic particles flattening, Surf. Coat. Technol., 200, 2005, p. 2317-2331.
12. A.A. Syed, A. Denoirjean, P. Denoirjean, J.C. Labbe, P. Fauchais, Invstigation of phenomena influencing properties of plasma sprayed ceramic-metal composite deposits, J. High Temp. Mater. Proc., Vol. 8 (2), 2004, 253- 272.
13. Schiller, R. Henne, M. Lang, R. Ruckdäschel, S. Schaper, Development of vacuum plasma sprayed thin-film SOFC for reduced operating temperature. Fuel Cells Bulletin, 21, 2000, p. 7-12.
14. DIN ISO 4022: Permeable sinter metals - evaluation of the specific permeability. Berlin, 1990 (in German)
15. Mould list; High porous sintered Bronze. Publication of GKN Sinter Metals, Radevormwald, Germany, 2005
16. A. Ansar, W. Richter, Z. Ilhan, Synthesis and properties of nanostructured SOFC anode deposits, J. High Temp. Mater. Proc., Vol. 11 (1), 2007, p 83 – 94.
17. H. Weckmann, A. Syed, Z. Ilhan, J. Arnold, Development of Porous Anode Layers for the Solid Oxide Fuel Cell by Plasma Spraying, J. Therm. Spray Technol., 15 (4), 2006, 604-609.
18. A. Ansar, Z.Ilhan, J. Arnold, Plasma sprayed metal supported SOFCs having enhanced performance and durability, accepted J. Therm. Spray. Technol., 2009.
19. C. Christenn, A. Ansar, Investigation of Plasma Sprayed and Constrained-Sintered Zirconia Based Electrolytes, accepted J. Therm. Spray. Technol., 2009.
20. P. Fauchais, V. Rat, J.-F. Coudert, R. Etchart-Salas, G. Montavon, Operating parameters for suspension and solution plasma-spray coatings, Surf. Coat. Technol., 202 (18), 2008, p. 4309-4317.
21. E. Brinley, K. S. Babu, S. Seal, The solution precursor plasma spray processing of nanomaterials, J. of the Minerals, 59 (7), 2007, p. 54-59.

22. F. Gitzhofer, L. Jia, Induction plasma technology applied to materials synthesis for SOFC, Int. J. Appl. Ceram. Technol., 5(6), 2008, p. 537-547.
23. T. Hofmann, Die Welt der vernachlässigten Dimensionen: Kolloide, Chem. Unserer Zeit, 38, 2004, p. 24.
24. G. Schiller, M. Müller, F. Gitzhofer, Preparation of Perovskite Powders and Coatings by Radio Frequency Suspension Plasma Spraying, J. Thermal Spray Techn. 8 (3), 1999, p 389-392.
25. M. Müller, E. Bouyer, M. v. Bradke, D. W. Branston, R. B. Heimann, R. Henne, G. Lins, G. Schiller, Thermal Induction Plasma Processes fort he Synthesis of SOFC Materials, Materialwissenschaft und Werkstoffkunde, 33 (6), 2002, p. 322-330